Effects of ion implantation and annealing on mechanical properties of ceramic using nanoindentor techniques

L. BOUDOUKHA, S. PALETTO, G. FANTOZZI
Groupe d'Etudes de Métallurgie Physique et Physique des Matériaux, URA 341, Bât. 502-INSA, F-69621 Villeurbanne cedex, France

F. HALITIM*
Institut de Chimie et Physique Industrielle, 31 Place Bellecour F-69288 Lyon cedex, France

Nanoindentor techniques have been used to obtain the values of hardness and elastic modulus of α-Al_2O_3 polycrystalline implanted with metallic species at room temperature with 170 keV, doses ranging from 2×10^{16} to 2×10^{17} ions cm^{-2}. After implantation, annealing was performed in the temperature range 600–1400 °C. An attempt has been made to correlate the mechanical property modifications with physico-chemical analysis. Elastic and plastic properties of the implanted layers, of about 100 nm thickness, have been characterized by microprobe investigation. This has indicated that certain fluences and thermal annealing temperatures are favourable for the improvement of mechanical properties.

1. Introduction

The use of ion implantation to modify the near surface properties of a hard ceramic such as Al_2O_3 has received increased attention in recent years [1–3]. Owing to the wide range of crystal structures, bonding characteristics, chemistry and mechanical properties of ceramics, a great diversity of ion implantation-induced modifications to mechanical properties is possible [4–6]. For instance, ion implantation into alumina may result in a radiation–solid solution hardened surface, a softened amorphized surface, or an apparently tougher surface [7]. A study has been conducted to determine modifications in the hardness and modulus of the implanted region by depth-sensing nanoindentation. In the present work, ion implantation was carried out on industrial polycrystalline α-alumina whose microscopic and macroscopic behaviour may strongly depend on the grain structure. Previous α-Al_2O_3 work has established that it is very difficult to make the near-surface region amorphous by ion implantation. Here we discuss the influence of thermal annealing on mechanical properties in the near-surface region.

2. Experimental procedure

2.1. Sample preparation

Ion implantations were performed on polycrystalline α-Al_2O_3 (Matroc, purity = 99.95%, mean grain size 3 μm). The samples were given a preliminary polish (average roughness 0.02 μm) and annealed in air for 1 h at 1200 °C, in order to remove the surface damage induced by mechanical polishing. Zirconium and copper ions were implanted at ambient temperature with an energy of 170 keV with doses in the range 10^{16} to 10^{17} ions cm^{-2}. Thermal annealing was carried out in air for 1 h at temperatures in the range 600–1400 °C. Table I gives a list of the ion species that have been implanted into α-Al_2O_3, the implantation conditions, and the annealing conditions.

TABLE I Species and conditions for ion implantation and annealing of α-Al_2O_3

Ion	Dose (ions cm^{-2})	Energy (keV)	Annealing (°C)
Zr	2×10^{16}	170	1000, 1200, 1400
	1×10^{17}		1000, 1200, 1400
	2×10^{17}		1000, 1200, 1400
Cu	2×10^{16}	170	600, 800, 1000
	1×10^{17}		600, 800, 1000

The choice of implanted species (zirconium and copper) was governed by the gap in the Gibbs energy of formation between alumina and the different oxides which are formed at specific annealing temperatures. The effects of implantation and annealing on the mechanical properties were evaluated using the nanoindentation technique and these results were correlated with the physical and structural property changes measured by Rutherford backscattering spectrometry (RBS), scanning electron microscopy (SEM) and grazing-angle X-ray diffraction (GXRD).

2.2. Nanoindentation technique

Load/displacement data were obtained by the nanoindentor technique (Nano Instruments, Inc.) [8–10].

0022–2461 © *1997 Chapman & Hall*

TABLE II Nanoindentation test sequence used in these experiments

Segment	Type of segment	Rate ($nm\,s^{-1}$)	Depth (nm)	Unloading %
1	Approach	10	–	–
2	Loading	5	20	–
3	Unloading	100%	–	90
4	Loading	5	45	–
5	Unloading	100%	–	90
6	Loading	5	60	–
7	Unloading	100%	–	90
8	Loading	5	90	–
9	Unloading	100%	–	90
10	Hold	100-s		
11	Unloading	100%	–	100

The instrument continuously monitors the displacement of an indentor by a capacitance gauge as load is applied. The displacement resolution is 0.04 nm and the loading force resolution is 75 nN. The measurements of hardness and modulus were obtained using a Berkovich triangular pyramid diamond with the same nominal area to depth relationship as the standard Vickers pyramid.

Tests were conducted at a constant indent displacement rate of $5\,nm\,s^{-1}$ by loading and unloading, producing depths in the range 0–100 nm. These depths were chosen with reference to the ion depth profile of the specimens. At each indent position, the sample was loaded to a specified depth, unloaded to a specified amount, and reloaded to a deeper depth several times according to the scheme shown Table II. The hardness and the Young's modulus at a depth of 45 nm are used for comparison, because this depth was almost the maximum depth profile of ion implantation. These mechanical properties were calculated using the true calibrated shape of the diamond [11]. The load–displacement curve of most ceramic materials resembles the curve shown in Fig. 1a, but the deformation mechanisms are very different from those observed in metallic materials such as aluminium (see Fig. 1b). The experimentally measured parameters required, to apply the model for calculation of hardness and modulus are the load on the indentor, P, the displacement of the indentor, and the stiffness determined by the slope of the initial portion of the unloading curve via a linear fit.

3. Results and discussion

Many measurements have been undertaken to explore the effects of ion implantation as a function of different treatment parameters. The presentation of our results will centre on annealing in air at different temperatures in comparison with implanted species and described doses. It should be noticed that the values obtained for some samples are very spread out. This could be related to the presence of grain boundaries, to the porosity and to the formation of various phases which probably display different hardnesses and moduli. Results of hardness and elastic modulus, given in percentages, compared to the unimplanted material

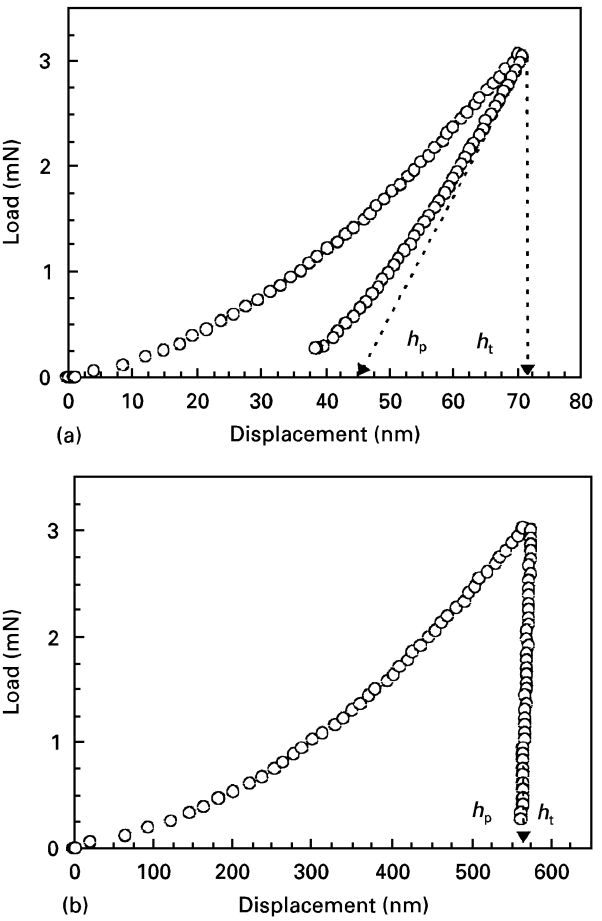

Figure 1 Load–displacement curves of (a) material that exhibits both elastic and plastic deformation, such as ceramics (alumina), (b) material that exhibits essentially no elastic deformation (aluminium) (h_p is the plastic depth, h_t the total displacement).

are the average of ten indentations for each sample measured at a depth of 45 nm.

3.1. Mechanical property changes in α-Al_2O_3 implanted with zirconium ions followed by thermal annealing

Fig. 2 shows the measured hardness and modulus change as a result of implantation with zirconium and after thermal annealing in air, carried out at 1000, 1200 and 1400 °C. For a low dose, 2×10^{16} ions cm^{-2}, zirconium ion implantation without annealing induces a decrease of about 57% in hardness. After implantation, the GXRD analysis shows that only the α-Al_2O_3 phase is detected, but the spectrum is disturbed, showing a high concentration of defects, thus explaining the decrease in hardness. Observations of specimens implanted to 2×10^{16} Zr ions cm^{-2} using X-ray photoelectron spectroscopy reveal a buried amorphous layer [12] and also explain the decrease in hardness. After annealing at 1000 °C, the hardness and the modulus increase but remain lower than those of the unimplanted alumina, GXRD shows that the only phase present is α-Al_2O_3, at the beginning of the recrystallization of the amorphous layer [13]. This corresponds to an increase of about 20% in hardness and 25% in Young's modulus, after annealing at 1200 °C, although the GXRD spectrum did identify

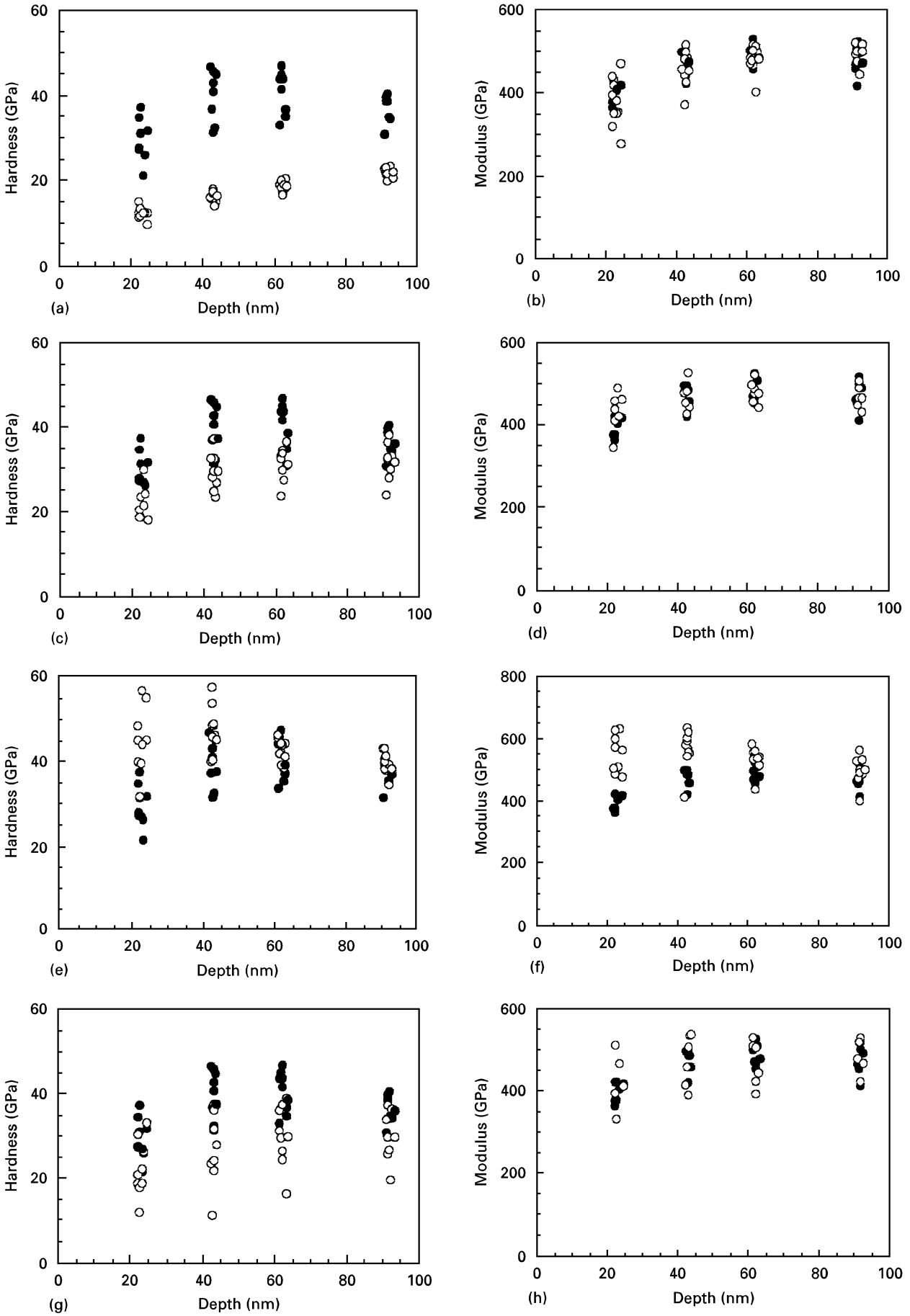

Figure 2 Evolution of mechanical properties versus depth ((a, c, e, g) hardness, (b, d, f, h) Young's modulus) for (●) unimplanted and (○) implanted alumina (2×10^{16} Zr ions cm^{-2}), followed by thermal annealing at (c, d) 1000 °C, (e, f) 1200 °C and (g, h) 1400 °C.

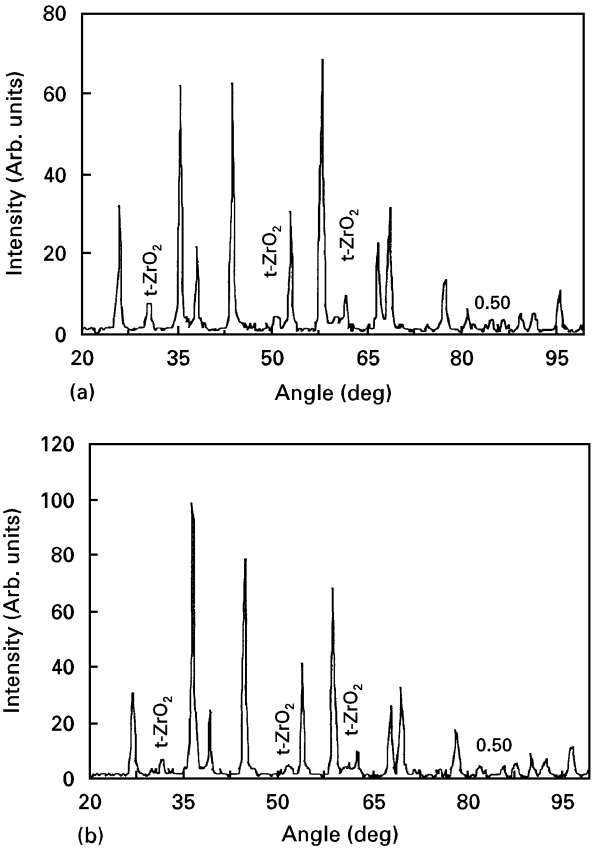

Figure 3 GXRD spectra of implanted alumina at 2×10^{16} Zr ions cm^{-2} and annealed at (a) 1200 °C or (b) 1400 °C.

small zirconia (ZrO_2) precipitates (see Fig. 3). The hardness and the modulus again decrease after annealing at 1400 °C. Rutherford back scattering (RBS) analysis shows that at this temperature there is an increase in surface zirconium concentration. This is clearly observed in the SEM as a form of superficial ZrO_2 precipitate, the GXRD spectrum also shows ZrO_2 rays (see Fig. 3). The presence of ZrO_2 produces a reduction in hardness and modulus over those of unimplanted alumina.

For the dose 1×10^{17} Zr ions cm^{-2}, decreases of about 60% for hardness and 15% for Young's modulus are observed in the sample implanted without annealing, with respect to unimplanted alumina (see Fig. 4). For this dose, GXRD analysis shows that the implantation produces amorphization of the implanted zone, explaining the decrease in the mechanical properties. Burnett and Page [14] show that implantation at a dose of 10^{17} ions cm^{-2} or above, at room temperature, would produce more amorphous Al_2O_3 in the near surface region. The amorphous layer could be detected by a decrease in the mechanical properties. At both annealing temperatures (1000 and 1200 °C), GXRD analysis clearly identifies tetragonal zirconia precipitates (t-ZrO_2) (see Fig. 5), the upper temperature induces an increase in the ZrO_2 ray intensity and shows that the tetragonal form is strongly deformed. The presence of ZrO_2 explains the decrease in hardness and modulus. The value of hardness remains lower than that of the unimplanted

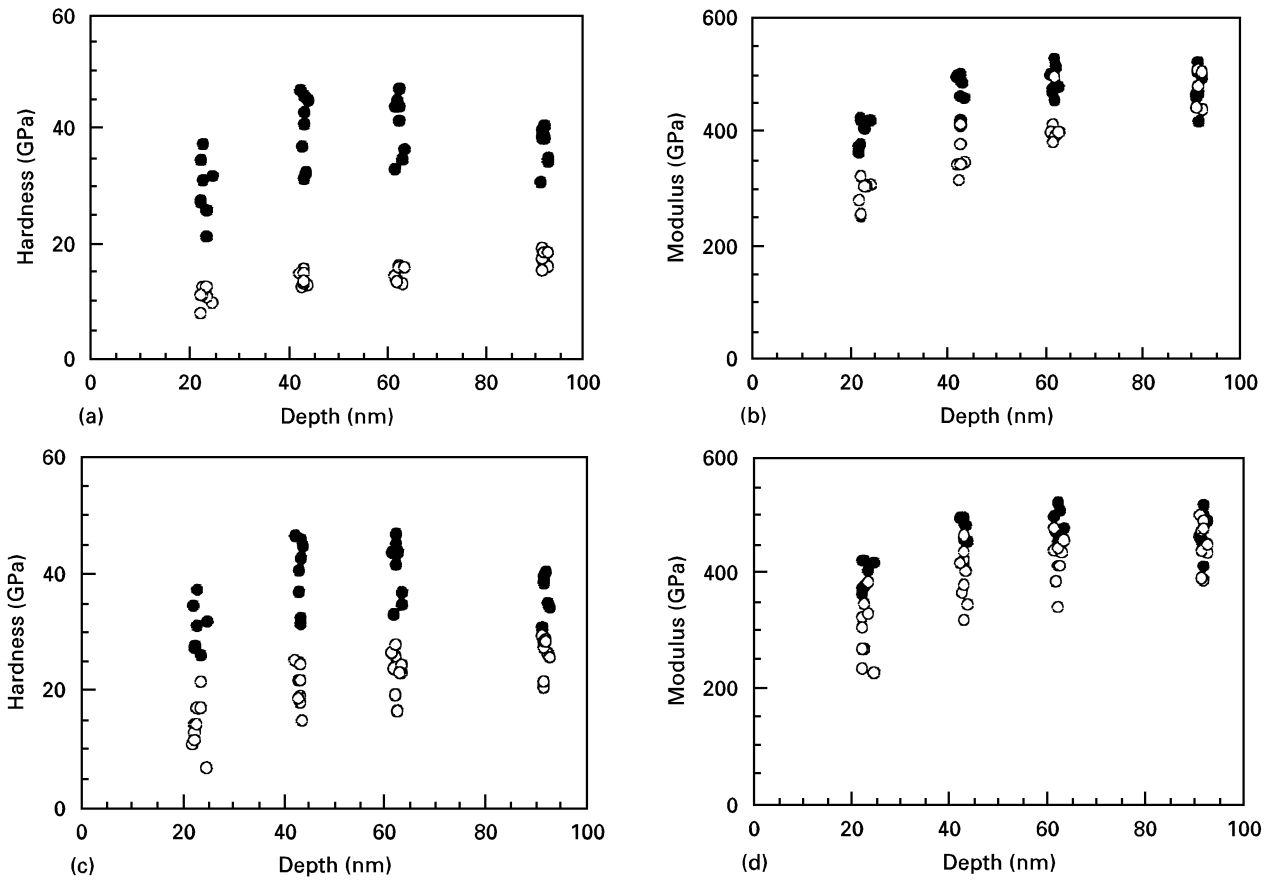

Figure 4 Evolution of mechanical properties versus depth ((a, c, e, g) hardness, (b, d, f, h) Young's modulus) for (●) unimplanted and (○) implanted alumina (1×10^{17} Zr ions cm^{-2}) followed by thermal annealing at (c, d) 1000 °C, (e, f) 1200 °C and (g, h) 1400 °C.

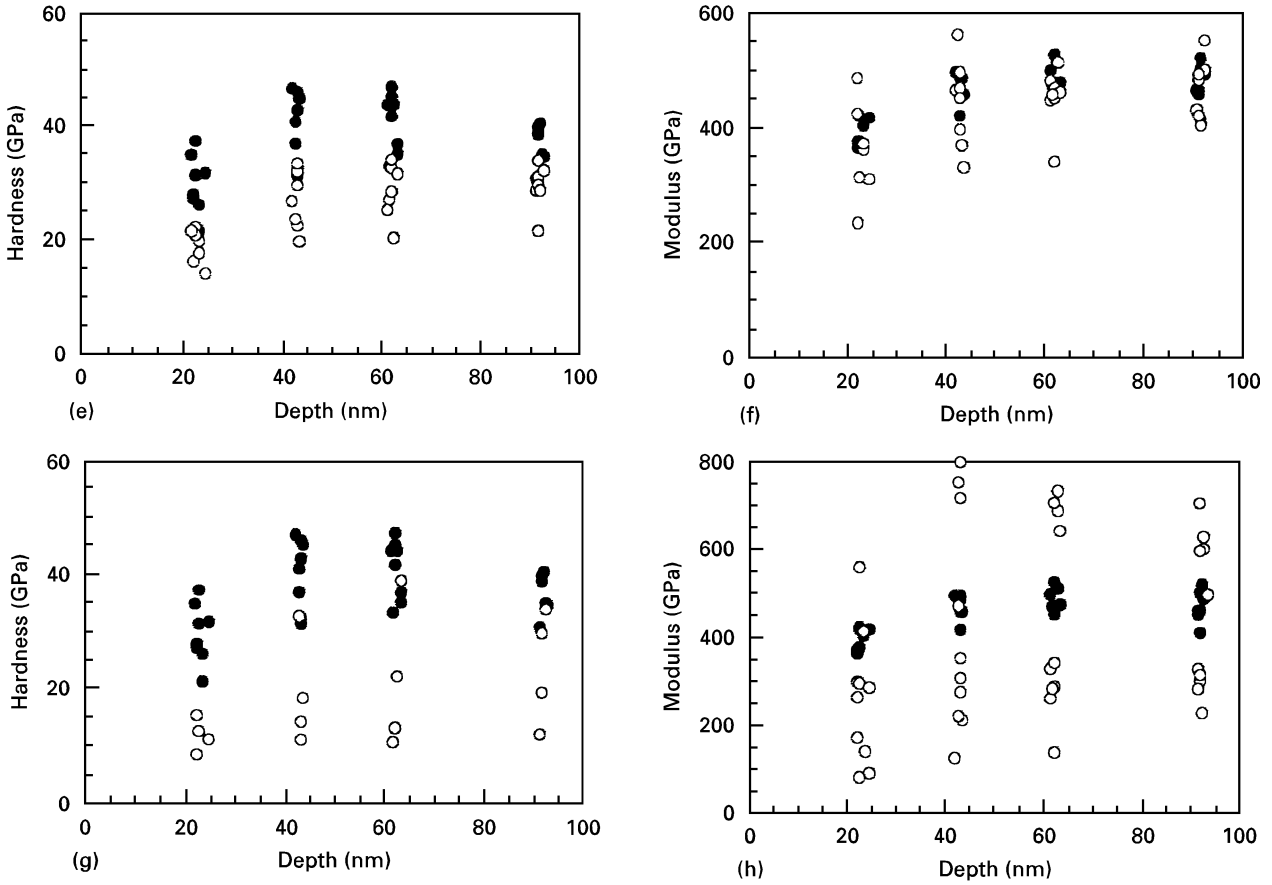

Figure 4 Continued.

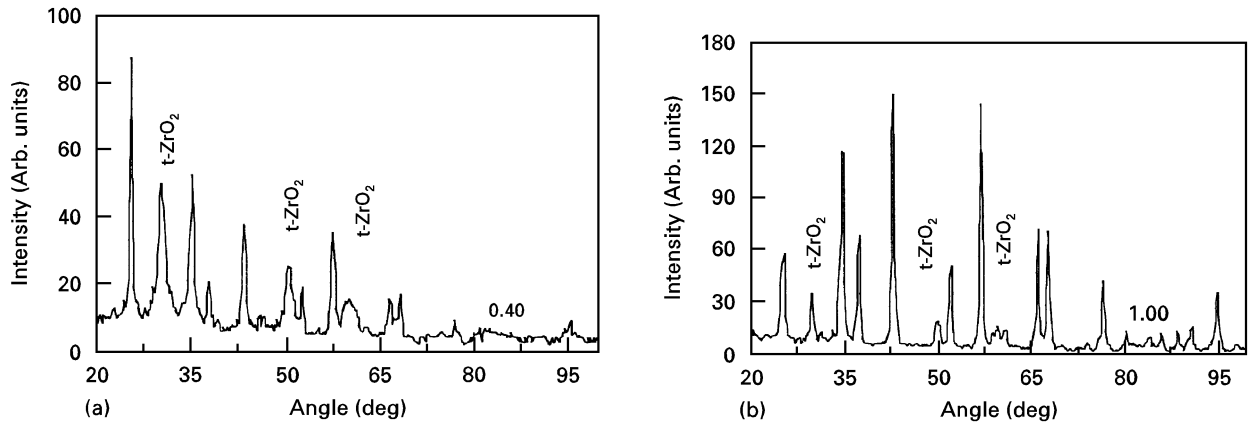

Figure 5 GXRD spectra of implanted alumina at 1×10^{17} Zr ions cm^{-2} and annealed at (a) 1000 °C or (b) 1200 °C.

alumina; after a thermal annealing at 1400 °C, the Young's modulus values are very spread out.

Similarly, for the higher dose, 2×10^{17} Zr ions cm^{-2}, after implantation and without annealing, decreases of about 60% hardness and 15% elastic modulus were found (see Fig. 6). The GXRD (see Fig. 7) spectrum indicates the presence of an amorphous phase, explaining the decrease in hardness and modulus. This behaviour is in agreement with results for other implanted ions [15, 16]. It has also been shown [17] that the hardness and elastic modulus decrease when the surface was made amorphous by stoichiometric implant of aluminium and oxygen at 77 K. After annealing at 1000 °C, the hardness and modulus remain lower than that of the unimplanted alumina. GXRD shows that t-ZrO_2 is observed, but with a stronger ray intensity, explaining the decrease of these parameters. For annealing at 1200 °C, the hardness remains lower than that of unimplanted alumina, but the Young's modulus returns to the initial value. GXRD analysis identified monoclinic zirconia precipitates (m-ZrO_2). At the higher temperature, 1400 °C, the mechanical parameters (H, E) remain lower than those of the unimplanted alumina. The presence of a higher zirconium concentration at the surface causes the decrease in hardness and

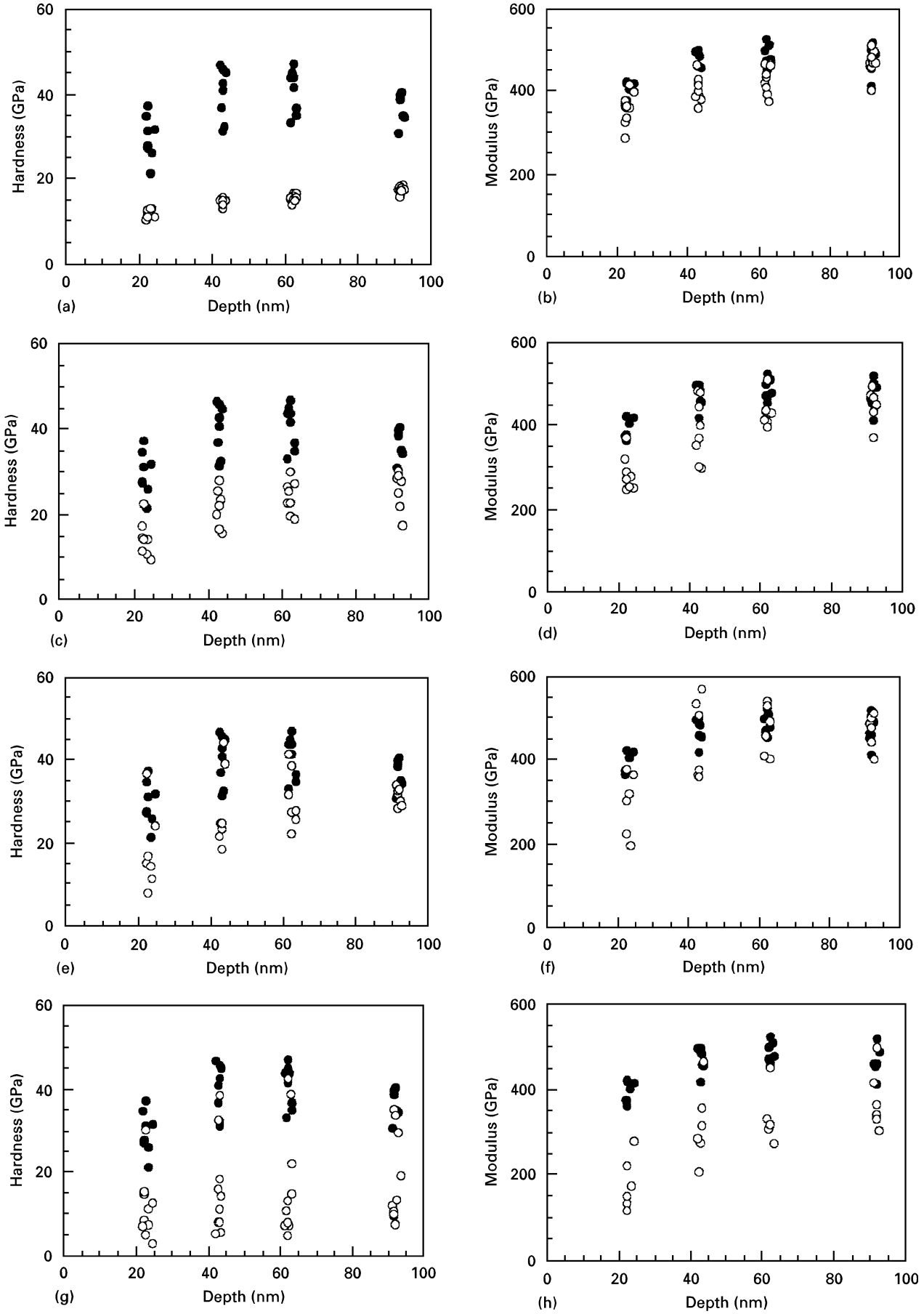

Figure 6 Evolution of the mechanical properties versus depth ((a, c, e, g) hardness, (b, d, f, h) Young's modulus) for (●) unimplanted and (○) implanted alumina (2×10^{17} Zr ions cm^{-2}) followed by thermal annealing at (c, d) 1000 °C, (e, f) 1200 °C and (g, h) 1400 °C.

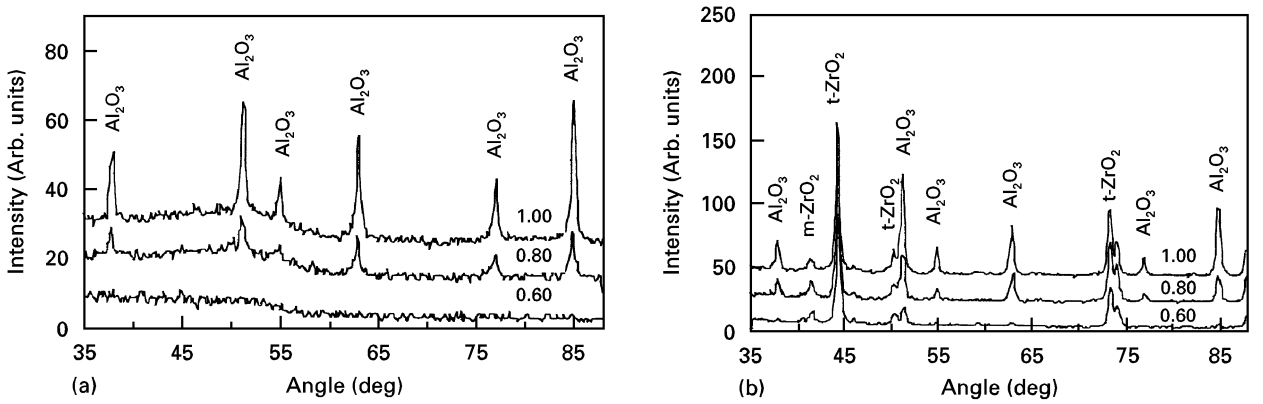

Figure 7 GXRD spectra of implanted alumina at 2×10^{17} Zr ions cm^{-2}, (a) implanted and (b) annealed at 1400 °C.

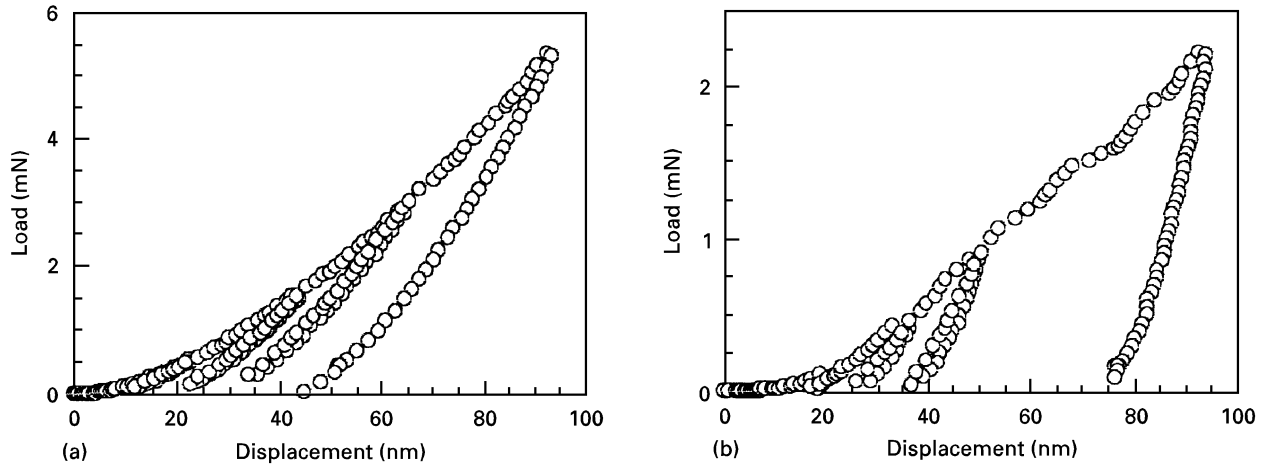

Figure 8 Load versus displacement for an experiment performed on (a) unimplanted alumina, and (b) alumina implanted at 2×10^{17} Zr ions cm^{-2}, annealed at 1400 °C.

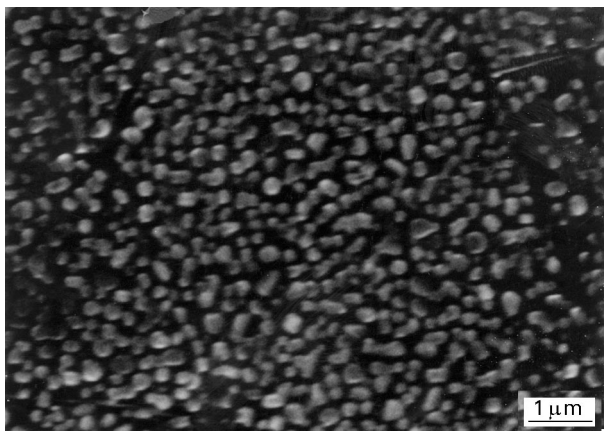

Figure 9 Scanning electron micrograph of zirconium-implanted alumina after annealing at 1400 °C.

modulus. At this temperature, a m-ZrO_2 is detected by GXRD (see Fig. 7) (less important at 1400 °C than at 1200 °C) and we observe a behaviour (plastic behaviour) entirely different from the unimplanted alumina (elastoplastic behaviour) (see Fig. 8). Other authors [18] have shown that the t-ZrO_2 to m-ZrO_2 transition is often observed in this temperature range, because the precipitate size becomes large enough to force crystallographic transition upon cooling. RBS shows that thermal annealing affects the zirconium concentration in the implanted zone. The zirconium ions come to the surface at 1400 °C where a higher concentration is observed by SEM (see Fig. 9).

3.2. Mechanical property changes in α-Al_2O_3 implanted with copper ions followed by thermal annealing

For a low dose, 2×10^{16} Cu ions cm^{-2}, the copper-ion implantation, without annealing, induces an increase of about 15% in the hardness and 9% in the modulus (see Fig. 10). This can be attributed to the formation of a solid-solution hardened region; GXRD analysis shows that only the α-Al_2O_3 phase is detected. After annealing at 600 °C, the hardness and the modulus remain unchanged from that of the unimplanted alumina. An increase of about 18% in hardness and 20% in modulus, after annealing at 800 °C, are observed with respect to the unimplanted alumina. It is associated with the formation of the precipitates, although the GXRD shows that the only phase present is α-Al_2O_3. These mechanical properties remain unchanged from the original unimplanted sample for annealing at 1000 °C.

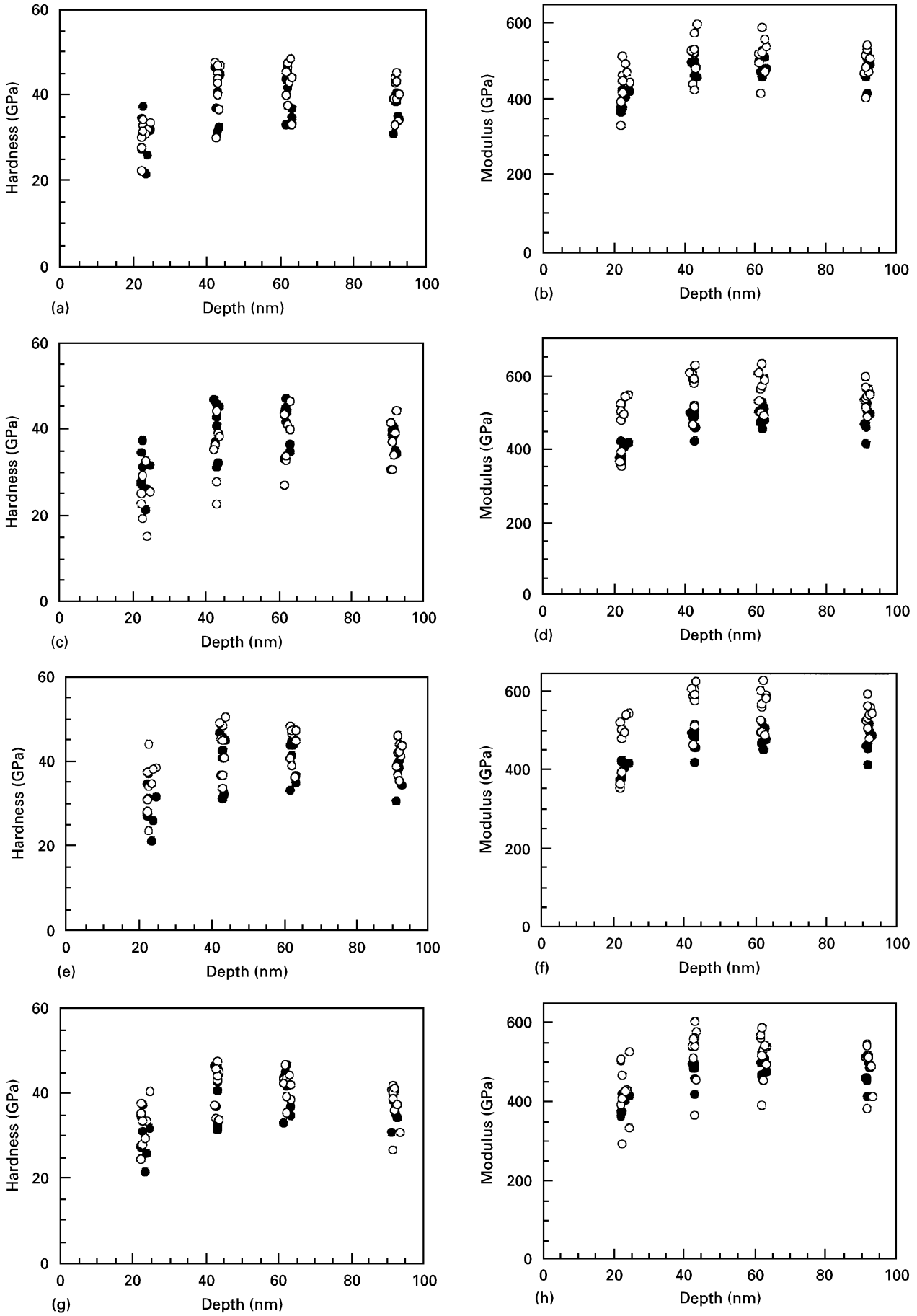

Figure 10 Evolution of mechanical properties versus depth ((a, c, e, g) hardness, (b, d, f, h) Young's modulus) for (●) unimplanted and (○) implanted alumina (2×10^{16} Cu ions cm^{-2}) followed by thermal annealing at (c, d) 600 °C, (e, f) 800 °C and (g, h) 1000 °C.

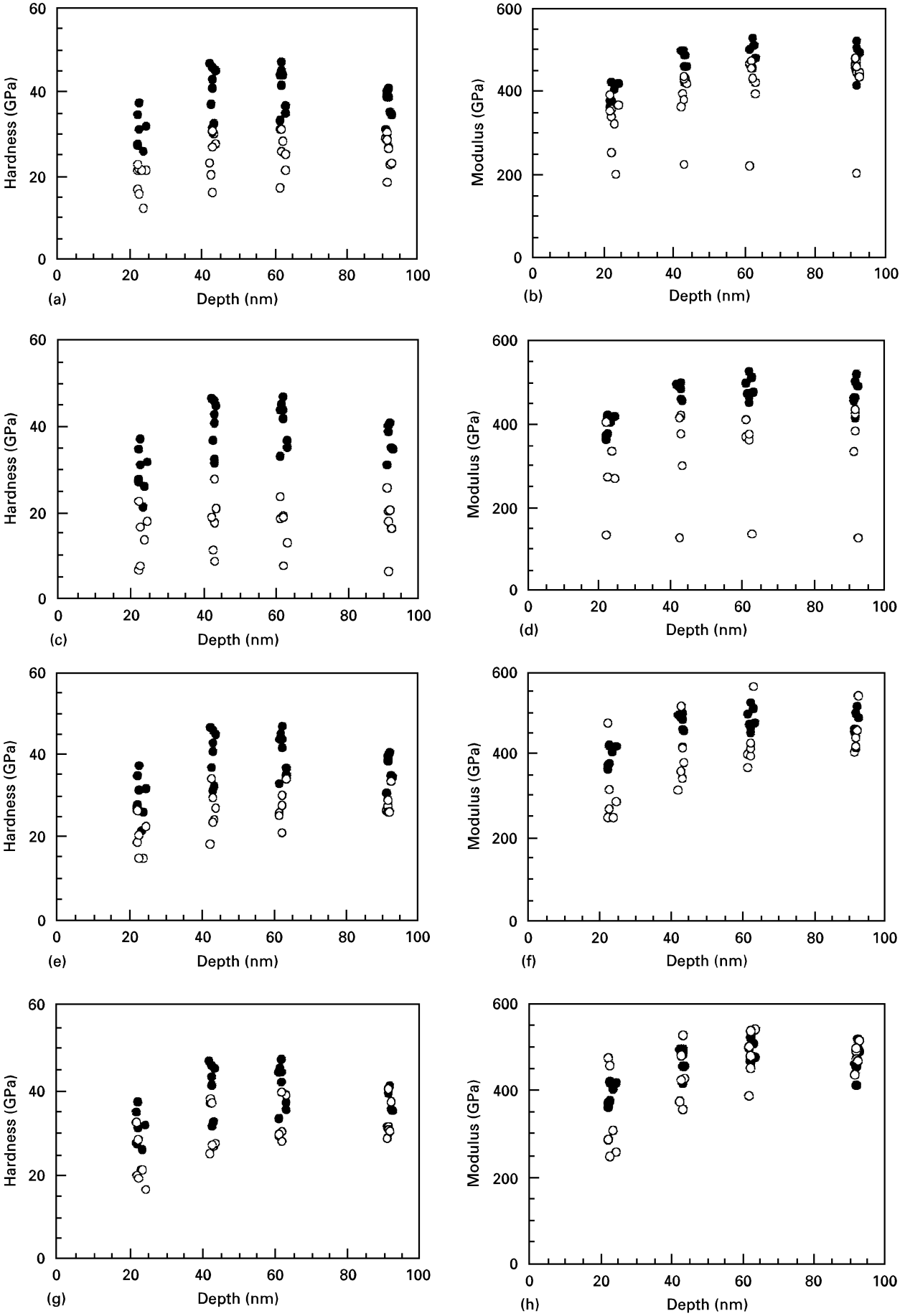

Figure 11 Evolution of mechanical properties versus depth ((a, c, e, g) hardness, (b, d, f, h) Young's modulus) for (●) unimplanted and (○) implanted alumina (1×10^{17} Cu ions cm^{-2}) followed by thermal annealing at (c, d) 600 °C, (e, f) 800 °C and (g, h) 1000 °C.

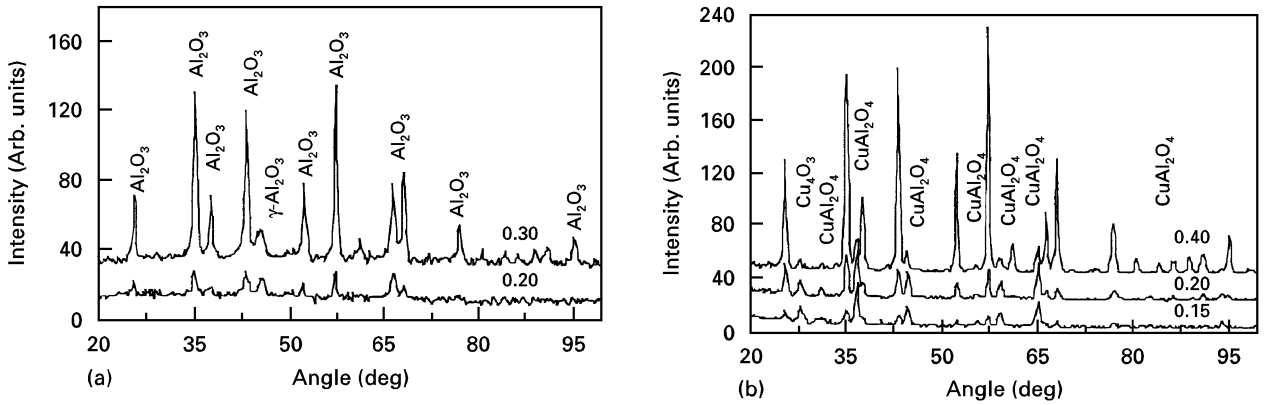

Figure 12 GXRD spectra of implanted alumina at 1×10^{17} Cu ions cm^{-2}, (a) implanted and (b) annealed at 1400 °C.

For the higher dose, 1×10^{17} Cu ions cm^{-2}, a decrease of about 30% in hardness and 13% in modulus is observed (see Fig. 11). In this critical dose, the microstructure is damaged but remains crystalline, and GXRD (see Fig. 12) shows the formation of γ-Al_2O_3. After annealing at 600 °C, the hardness and the modulus decrease compared to that of the unimplanted alumina. The GXRD spectrum indicates the presence of the monoclinic copper oxide, CuO, mixed with γ-Al_2O_3. The mechanical properties remain lower than those of the unimplanted alumina, for annealing at 800 and 1000 °C. Annealing at these temperatures induces the formation of the spinel phase $CuOAl_2O_4$ (see Fig. 12).

4. Conclusion

It has been shown that ion implantation of zirconium and copper into polycrystalline α-Al_2O_3 results in substantial changes in surface mechanical properties relative to the unimplanted state, this is characterized by a depth-sensing low-load indentation technique. An amorphous-like layer is detected in the case of zirconium implantation with a tendency to form zirconia crystals, and the hardness and the Young's modulus of the implanted alumina are lower than those of the unimplanted samples. During thermal annealing, the zirconium is entirely oxidized in the form of tetragonal and then monoclinic ZrO_2 phases, and a significant increase in hardness and modulus is observed after annealing at 1200 °C with a low dose. The implanted alumina retains its crystallinity in the case of copper implantation and the mechanical properties increase in comparison with the original unimplanted material. Thermal treatments lead to the formation of surface copper oxide and spinel precipitates. Results show that with low-dose ion implantation followed by annealing at a temperature of 800 °C, these mechanical properties increase, possibly due to precipitation hardening.

The results presented clearly show the ability of nanoindentation to measure changes in the mechanical properties of polycrystalline implanted α-alumina. Further investigations are necessary to study the effects of zirconium and copper ions on tribological properties (wear and friction coefficient).

Acknowledgements

We thank Direction des Recherches Etudes Techniques for their financial support. We are also very grateful to J. Bigarre who performed GXRD tests.

References

1. K. FUKUMI, A. CHAYAHARA, M. MAKIHARA, K. FUJII, J. HAYAKAWA and M. SATOU, *J. Amer. Ceram. Soc.* **77** (1994) 3019.
2. S. J. BULL and T. F. PAGE, *J. Mater. Sci.* **26** (1991) 3086.
3. M. E. O'HERN, C. J. McHARGUE, C. W. WHITE and G.C. FARLOW, *Nucl. Instrum. Meth. Phys. Res.* **46** (1990) 171.
4. C. J. McHARGUE, *ibid.* **19/20** (1987) 797.
5. T. HIOKI, A. ITOH, M. OHKUBO, S. NODA, H. DOI, J. KAWAMOTO and O. KAMIGAITO, *ibid.* **21** (1986) 1321.
6. T. HIOKI, A. ITOH, S. NODA, H. DOI, J. KAWAMOTO and O. KAMIGAITO, *ibid.* **7/8** (1985) 521.
7. P. J. BURNETT and T. F. PAGE, *Rad. Effects* **97** (1986) 283.
8. J. B. PETHICA, R. HUTCHINGS and W. C. OLIVER, *Philos. Mag.* **48** (1983) 593.
9. D. L. JOSLIN and W. C. OLIVER, *J. Mater. Res.* **5** (1990) 123.
10. W. C. OLIVER, G. M. PHARR, *ibid.* **7** (1992) 1564.
11. L. BOUDOUKHA, S. PALETTO and G. FANTOZZI, *Nucl. Instrum Meth. Phys. Res.* **108** (1996) 87.
12. C. W. WHITE, G. C. FARLOW, C. J. McHARGUE, P. ANGELINI, P. S. SKLAD, M. B. LEWIS and B. R. APPLETON, *ibid.* **7/8** (1985) 473.
13. H. NARAMOTO, C. J. McHARGUE, C. W. WHITE, J. M. WILLIAMS, O. W. HOLLAND, M. M. ABRAHAM, and B. R. APPLETON, *J. Appl. Phys.* **210** (1983) 1159.
14. P. J. BURNETT and T. F. PAGE, *J. Mater. Sci.* **22** (1984) 3524.
15. *Idem*, *Amer. Ceram. Soc. Bull.* **10** (1986) 1393.
16. N. MONCOFFRE, *Nucl. Instrum. Meth. Phys. Res.* **59/60** (1991) 1129.
17. W. C. OLIVER, C. J. McHARGUE, S. J. ZINKLE. *Thin Solids Films* **153** (1987) 185.
18. C. DONNET, G. MAREST, N. MONCOFFRE, J. TOUSSET, A. RAHIOUI, C. ESNOUF and M. BRUNEL, *Nucl. Instrum. Meth. Phys. Res.* **59/60** (1991) 1205.

Received 5 June 1996
and accepted 7 January 1997